Inorganic Chemistry

Article

pubs.acs.org/IC

Multifunctional Uranyl Hybrid Materials: Structural Diversities as a Function of pH, Luminescence with Potential Nitrobenzene Sensing, and Photoelectric Behavior as *p*-type Semiconductors

Jian Song,[†] Xue Gao,[†] Zhi-Nan Wang,[†] Cheng-Ren Li,[‡] Qi Xu,[‡] Feng-Ying Bai,[§] Zhong-Feng Shi,[⊥] and Yong-Heng Xing*[,†]

[†]College of Chemistry and Chemical Engineering, [‡]College of Physics and Electronic Technology, and [§]College of Life Sciences, Liaoning Normal University, Dalian 116029, P.R. China

[⊥]College of Chemistry and Chemical Engineering, Qinzhou University, Qinzhou 535099, P.R. China

Supporting Information

ABSTRACT: A series of uranyl−organic frameworks (UOFs), $\{[(UO_2)_2(H_2TTHA)(H_2O)]\cdot 4,4'\text{-bipy}\cdot 2H_2O\}_n$ (**1**), $\{[(UO_2)_3(TTHA)(H_2O)_3]\}_n$ (**2**), and $\{[(UO_2)_5(TTHA)(HTTHA)(H_2O)_3]\cdot H_3O\}_n$ (**3**), have been obtained by the hydrothermal reaction of uranyl acetate with a flexible hexapodal ligand (1,3,5-triazine-2,4,6-triamine hexaacetic acid, H_6TTHA). These compounds exhibited three distinct 3D self-assembly architectures as a function of pH by single-crystal structural analysis, although the used ligand was the same in each reaction. Surprisingly, all of the coordination modes of the H_6TTHA ligand in this work are first discovered. Furthermore, the photoluminescent results showed that these compounds displayed high-sensitivity luminescent sensing functions for nitrobenzene. Additionally, the surface photovoltage spectroscopy and electric-field-induced surface photovoltage spectroscopy showed that compounds **1**−**3** could behave as *p*-type semiconductors.

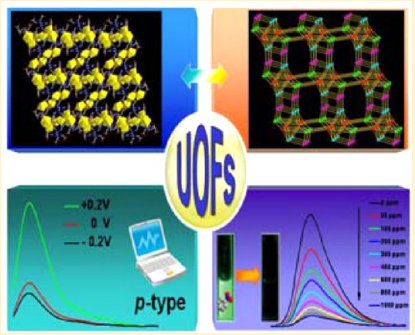

INTRODUCTION

Metal−organic frameworks (MOFs)[1a,b] have attracted increasing attention because of their remarkable potential applications in gas storage,[1c,d] adsorption and separation,[2] biomedical imaging,[3] magnetic,[4] luminescence sensors,[5] and sensors over light-emitting devices (LEDs, OLEDs).[6] In contrast to the huge amount of 3d and 4f metal−organic frameworks, 5f actinide compounds that adopt various topologies and coordination geometries have been less investigated. In recent years, the chemistry of actinide-bearing hybrid materials has become more and more seductive in consideration of their importance in nuclear waste management and separation processes.[7] In this course, uranyl−organic assemblies have received considerable attention not only because of their diverse chemical compositions and architectures but also a wide range of important physicochemical properties that include ion exchange, ionic conductivity, intercalation chemistry, photochemistry, nonlinear optics, and selective oxidation catalysis.[8−10] The coordination chemistry of uranium is dominated by U^{VI}, in the form of uranyl cation $[UO_2]^{2+}$, a peculiar linear triatomic species capped with terminal oxygen atoms.[11] When it is associated with O-donor ligands (i.e., multidentate carboxylates), uranium exhibits an interesting chemical ability to successfully form an abundant variety of frameworks with different network dimensionalities through 4−6 additional coordination sites in the equatorial plane (4 + 2, square bipyramid; 5 + 2, pentagonal bipyramid; 6 + 2, hexagonal bipyramid).[12] Until now, the so-called uranyl−organic frameworks (UOFs) have been described in many contributions with the use of aliphatic or aromatic polydentate carboxylates, which may also incorporate heterogroups such as nitrogen- or sulfur-donor functions.[13] Among these structures, the construction of 3D uranyl frameworks is relatively lacking but highly desirable.[14] Three-dimensional UOFs usually exhibit superior thermal stability to low-dimensional structures and many outstanding properties, such as photoelectric effects,[14a] nonlinear optical properties,[14h] and porous adsorption.[14i]

It is well-known that modification of the organic component of hybrid materials further contributes to structural variation.[15] One popular strategy to produce the self-assembly of 3D UOFs is to employ highly symmetrical multidentate ligands containing poly(carboxylic acid) groups as per their affinity for $[UO_2]^{2+}$. Previously, some flexible polypodal ligands, such as, *N*,*N*′,*N*″-1,3,5-triazine-2,4,6-triyltris-glycine (TTG),[16] 2,2′,2″-[1,3,5-triazine-2,4,6-triyltris(thio)]tris-acetic acid (TTTA),[17] and tris(2-carboxyethyl)isocyanurate (H_3TCI),[18] leading to novel compounds with unusual characters and topologies have been reported. Afterwards, another intriguing organic ligand, 1,3,5-triazine-2,4,6-triamine hexaacetic acid (H_6TTHA, Scheme 1), has attracted our attention. H_6TTHA has a planar triazine core with three symmetrically placed metal-compounding flexible aminodiacetate arms. Comparing it with the traditional rigid ligands, it can adopt multiple

Received: June 17, 2015
Published: September 2, 2015

DOI: 10.1021/acs.inorgchem.5b01364
Inorg. Chem. 2015, 54, 9046−9059

Scheme 1. Molecular Structure of H_6TTHA

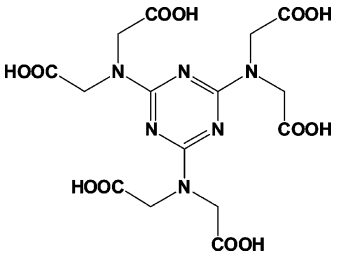

conformations and bonding modes to meet the geometrical requirements of the central metal ions, e.g., *syn-syn*, *anti-anti*, *syn-anti*, and monomonodentate and monobidentate, and so forth,[19] which result in a variety of structural frameworks. Several coordination polymers related to ligand H_6TTHA with a wide variety of metal ions, such as Na, Mg, Cu, Zn, and so on, have been reported, which display versatile conformations and coordination modes.[19,20] It becomes imperative to explore more, different structural landscapes of multicomponent systems consisting of metal ions and the flexible ligand H_6TTHA to understand factors governing their aggregation in different crystallization conditions. Meanwhile, some of these compounds based on the ligand H_6TTHA were found to exhibit a variety of outstanding properties. For example, Zhu and co-workers constructed a series of 3d and 4f CPs with microporous structures, excellent fluorescent emissions, antiferromagnetic interactions, and gas storage behaviors.[19a,b] Then, they prepared five Cd^{II} and Zn^{II} compounds, which exhibited unusual luminescence thermochromism, reversible radical-based redox photochromism varying from yellow to bluish violet and dark blue, respectively, and fluorescence with adjustable intensity.[20a,c] Zhang et al. reported one novel 3d−4f microporous heterometal−organic framework (HMOF) with high-sensitivity luminescent sensing functions for BTEX (benzene, toluene, ethylbenzene, xylenes), particularly for ethylbenzene.[20g] Thus, our attention has also focused on constructing 3D UOFs with outstanding properties based on 1,3,5-triazine-2,4,6-triamine hexaacetic acid.

As one of the important chemical intermediates, nitrobenzene has been widely used for dyes, pharmaceuticals, and pesticides.[21] It is also a well-known explosive and highly toxic contaminant with a broad range of detriments.[22] Usually, canines and sophisticated instrumental methods are used to detect nitrobenzene, but these methods are inconvenient and not always available.[23] Therefore, the sensitive and selective detection of nitrobenzene is very necessary. To date, some luminescent MOFs for sensing nitrobenzene have been reported.[24] For example, Guo et al. reported a high sensitivity luminescent MOF, $Zn_3(L1)_2(L2)$ {L1 = 4-[3-(4-carboxyphenoxy)-2-[(4-carboxyphenoxy)methyl]-2-methyl-propoxy]-benzoate, L2 = 1,4-bis(1-imidazolyl)benzene]}, which quenched at 50 ppm with a high quenching efficiency of 98.91%. To the best of our knowledge, it is the most sensitive nitrobenzene detector at present.[24i] The origin of these working mechanisms is considered to arise from the electron-withdrawing properties of nitro groups contained in the analytes, hence, the significant donor−acceptor electron transfer from ligands to electron-donating MOF structures. For other fields, Chen et al. reported a 3D heterobimetallic uranyl−zinc carboxylate and investigated the surface photoelectric properties. The results demonstrated well that this uranyl compound could behave as an *n*-type semiconductor.[14a] Gao et al. and Liao et al. also reported a series of uranyl compounds, which all exhibited excellent photoelectric properties.[14j,k] We have also attempted to detect these properties for the uranyl compounds, which may impel more developments of uranyl compounds as multifunctional materials.

Herein, we present a family of hydrothermally synthesized 3D uranyl hybrid materials incorporating the flexible polycarboxylate ligand H_6TTHA: $\{[(UO_2)_2(H_2TTHA)(H_2O)]\cdot 4,4'\text{-bipy}\cdot 2H_2O\}_n$ (**1**), $\{[(UO_2)_3(TTHA)(H_2O)_3]\}_n$ (**2**), and $\{[(UO_2)_5(TTHA)(HTTHA)(H_2O)_3]\cdot H_3O\}_n$ (**3**). To the best of our knowledge, no crystal structures of uranyl compounds with 1,3,5-triazine-2,4,6-triamine hexaacetic acid have been reported to date. In addition, we focus on the resulting local and global structural diversities of **1**−**3** as influenced by the pH and almost exhibit all of the conformations and coordination modes of the ligand H_6TTHA in the relevant reports. It is found that the coordination modes of the ligand H_6TTHA in this work are novel. Furthermore, the photoluminescent (PL) sensing property for nitrobenzene and the encouraging surface photoelectric properties [surface photovoltage spectroscopy (SPS) and electric-field-induced surface photovoltage spectroscopy (EFISPS)] are investigated in detail.

EXPERIMENTAL SECTION

Caution! *Although all of the uranyl compounds used in these studies contained depleted uranium salts, standard precautions were performed for handling radioactive materials, and all studies were conducted in a laboratory dedicated to studies on actinide elements.*

Materials and Methods. All chemicals purchased commercially were of reagent grade or better and used without further purification. Lanthanide nitrate salts were prepared via dissolving lanthanide oxides with 12 M HNO_3 and then evaporating at 100 °C until the crystal film formed. Elemental analyses of C, H, and N were conducted on a PerkinElmer 240C automatic analyzer at the analysis center of Liaoning Normal University. All IR measurements were obtained using a Bruker AXS TENSOR-27 FT-IR spectrometer with pressed KBr pellets in the range of 400−4000 cm^{-1} at room temperature. UV−vis−NIR spectra for three compounds, $UO_2(CH_3COO)_2\cdot 2H_2O$ and the H_6TTHA ligand, were recorded on a JASCO V-570 UV/vis/NIR microspectrophotometer (200−2500 nm, in the form of a solid sample). Thermogravimetric analysis (TG) was performed on a PerkinElmer Diamond TG/DTA under atmosphere from room temperature to 1000 °C with a heating rate of 10 °C/min. X-ray powder diffraction patterns were obtained on a Bruker Advance-D8 equipped with Cu Ka radiation in the range $5° < 2\theta < 55°$ with a step size of 0.02° (2θ) and a count time of 2 s/step. The photoluminescent properties of compounds **1**−**3** were measured in the solid state and in different solvent emulsions on a JASCO FP-6500 spectrofluorimeter at room temperature. Surface photovoltage spectroscopy (SPS) and electric-field-induced surface photovoltage spectroscopy (EFISPS) measurements were conducted on a powdered sample in a sandwich cell (ITO/sample/ITO) with the light source-monochromator-lock-in detection technique, as illustrated in Figure S1. The electrode is made of optical glass coated with indium and tin oxides (ITO). Standard *p*-type silicon flakes were used to adjust the comparative phase, and a xenon lamp was used as an illuminator to supply radiation in the range of 300−800 nm.

Synthesis. The ligand 1,3,5-triazine-2,4,6-triamine hexaacetic acid (H_6TTHA) was synthesized according to the method described in the literature.[20a,25]

*$\{[(UO_2)_2(H_2TTHA)(H_2O)]\cdot 4,4'\text{-bipy}\cdot 2H_2O\}_n$ (**1**).* Compound **1** was synthesized by combining $UO_2(CH_3COO)_2\cdot 2H_2O$ (0.084 g, 0.2 mmol), $Nd(NO_3)_3\cdot 6H_2O$ (0.0438g, 0.1 mmol), H_6TTHA (0.0474g, 0.1 mmol), 4,4′-bipy (0.0312g, 0.2 mmol), and demineralized water (6 mL) in a glass vessel and stirring for 1 h at room temperature. Several drops (0.16 mL) of 4 M HNO_3 were added after dissolution of the

DOI: 10.1021/acs.inorgchem.5b01364
Inorg. Chem. 2015, 54, 9046−9059

Table 1. Summary of Crystal Data and Refinement Results for H_6TTHA and Compounds 1−3

	H_6TTHA	1	2	3
chemical formula	$C_{15}H_{18}N_6O_{12}$	$C_{25}H_{28}N_8O_{19}U_2$	$C_{15}H_{18}N_6O_{21}U_3$	$C_{30}H_{34}N_{12}O_{38}U_5$
M (g mol^{-1})	474.35	1220.61	1332.44	2360.84
crystal system	monoclinic	monoclinic	monoclinic	triclinic
space group	$C2/c$	$P2_1/n$	$P2_1/c$	P
a (Å)	5.0686(13)	11.460(4)	12.624(5)	14.533(3)
b (Å)	21.661(6)	19.968(6)	15.891(6)	15.479(4)
c (Å)	17.452(4)	14.949(5)	16.585(7)	15.666(4)
α (deg)	90	90	90	74.643(4)
β (deg)	91.591(5)	99.628(5)	105.217(6)	74.576(4)
γ (deg)	90	90	90	81.431(4)
V (Å^3)	1915.3(9)	3372.8(18)	3210(2)	3264.2(13)
Z	4	4	4	2
D_{calc} (mg m^{-3})	1.645	2.404	2.757	2.402
crystal size (mm)	0.35 × 0.24 × 0.10	0.45 × 0.32 × 0.29	0.45 × 0.36 × 0.10	0.52 × 0.36 × 0.25
F(000)	984	2280	2376	2124
μ(Mo Kα)/mm^{-1}	0.144	9.687	15.186	12.458
θ (deg)	1.88−28.28	1.72−25.00	2.22−25.00	1.46−25.00
reflections collected	5920	17062	15751	16508
independent reflections	2321 (1373)	5940 (4972)	5641 (4571)	11416 (8573)
parameters	154	489	406	766
R_{int}	0.0392	0.0301	0.0498	0.0264
$\Delta(\rho)$ (e Å^{-3})	0.168 and −0.205	1.750 and −0.568	2.839 and −2.583	5.365 and −2.042
goodness of fit	1.006	1.038	1.040	1.095
R^a	0.0483 (0.1000)[b]	0.0256 (0.0357)[b]	0.0428 (0.1232)[b]	0.0549 (0.1707)[b]
wR_2[a]	0.0908 (0.1076)[b]	0.0561 (0.0580)[b]	0.0559 (0.1304)[b]	0.0760 (0.1801)[b]

[a]$R = \Sigma||F_o| - |F_c||/\Sigma|F_o|$; $wR_2 = [\Sigma w(F_o^2 - F_c^2)^2/\Sigma w(F_o^2)^2]^{1/2}$; $|F_o| > 4\sigma(|F_o|)$. [b]On the basis of all of the data.

reactants. The light-yellow clear solution with a pH of ∼2.0 was transferred to a 23 mL Teflon-lined stainless steel autoclave and heated statically at 160 °C for 3 days and then allowed to crystallize over 2 days at room temperature. Unexpectedly, a mixture of yellow and light-purple single crystals was obtained from the colorless resulting solution with a pH of ∼3.0. The target product, yellow single crystals, were isolated with a yield of 65% based on $[UO_2]^{2+}$ after filtration and washing thoroughly with distilled water. Meanwhile, the light-purple crystals of the byproduct were proven to be the compound $[Nd(ox)_{1.5}(H_2O)_3]$ (ox = oxalic acid) resulting from in situ reaction of H_6TTHA into oxalic acid with a low yield of 10% based on Nd^{3+}. Elemental Analysis (%) Calcd for $C_{25}H_{28}N_8O_{19}U_2$: C, 24.60; H, 2.31; N, 9.18. Found: C, 24.75; H, 2.22; N, 9.06.

{[(UO$_2$)$_3$(TTHA)(H$_2$O)$_3$]}$_n$ (2). Compound **2** was synthesized by combining $UO_2(CH_3COO)_2{\cdot}2H_2O$ (0.042 g, 0.1 mmol), H_6TTHA (0.0237 g, 0.05 mmol), and demineralized water (6 mL) in a glass vessel and stirring for 1 h at room temperature. Several drops (0.12 mL) of 4 M HNO_3 were added after dissolution of the reactants. The light-yellow clear solution with a pH of ∼1.5 was transferred to a 23 mL Teflon-lined stainless steel autoclave and heated statically at 160 °C for 3 days and then allowed to crystallize over 2 days at room temperature. Yellow single crystals were obtained from the colorless resulting solution with a pH of ∼2.0, which could be isolated with a yield of 45% based on $[UO_2]^{2+}$ after filtration and washing thoroughly with distilled water. Elemental Analysis (%) Calcd for $C_{15}H_{18}N_6O_{21}U_3$: C, 13.52; H, 1.36; N, 6.31. Found: C, 13.35; H, 1.24; N, 6.45.

{[(UO$_2$)$_5$(TTHA) (HTTHA)(H$_2$O)$_3$]·H$_3$O}$_n$ (3). Compound **3** was synthesized by combining $UO_2(CH_3COO)_2{\cdot}2H_2O$ (0.042 g, 0.1 mmol), H_6TTHA (0.0237 g, 0.05 mmol), and demineralized water (6 mL) in a glass vessel and stirring for 1 h at room temperature. Several drops (0.08 mL) of 4 M HNO_3 were added after dissolution of the reactants. The light-yellow clear solution with a pH of ∼1.8 was transferred to a 23 mL Teflon-lined stainless steel autoclave and heated statically at 160 °C for 3 days and then allowed to crystallize over 2 days at room temperature. Yellow single crystals were obtained from the colorless resulting solution with a pH of ∼2.5, which could be isolated with a yield of 60% based on $[UO_2]^{2+}$ after filtration and washing thoroughly with distilled water. Elemental Analysis (%) Calcd for $C_{30}H_{34}N_{12}O_{38}U_5$: C, 15.26; H, 1.45; N, 7.12. Found: C, 15.19; H, 1.53; N, 7.01.

X-ray Crystal Structure Determination. Single crystals of suitable dimensions for the ligand H_6TTHA and compounds **1**−**3** were mounted on glass fibers for the X-ray structure determinations. Reflection data were collected at room temperature on a Bruker AXS SMART APEX II CCD diffractometer with graphite monochromatized Mo Kα radiation (λ = 0.71073 Å). A semiempirical absorption correction was applied by the program SADABS.[26] The program suite SHELXTL-97 was used for space-group determination (XPREP), direct method structure solution (XS), and least-squares refinement (XL).[27] All non-hydrogen atoms were refined with anisotropic displacement parameters. The positions of the hydrogen atoms around the carbon atoms were included using a riding model. The hydrogen atoms bound to oxygen atoms from the aqua molecules and the carboxylate groups were found on Fourier difference maps. For compound **3**, the uncoordinated carboxylate group (C30, O36, O37) of the ligand 1,3,5-triazine-2,4,6-triamine hexaacetic acid was too disordered to be fixed at calculated positions in the process of the structure refinement. The relevant hydrogen atom bound to O37 was not found on a Fourier-difference map. Restraints on bond lengths and/or displacement parameters were applied for poorly behaving atoms. The ISOR command had been used to refine the ADP of O1w in compound **3**. Some voids in the lattice likely indicate the presence of unresolved water solvent molecules, probably highly disordered.

Crystal data and structure refinement parameters are given in Table 1 and selected bond lengths and angles of compounds **1**−**3** are listed in Table S1.

RESULTS AND DISCUSSION

Synthesis. With the aim of synthesizing various uranyl compounds possessing intriguing uranyl−organic frameworks (UOFs), we designed reactions of uranyl acetate and a flexible hexapodal ligand, 1,3,5-triazine-2,4,6-triamine hexaacetic acid (H_6TTHA), under various experimental conditions. A new

DOI: 10.1021/acs.inorgchem.5b01364
Inorg. Chem. 2015, 54, 9046−9059

family of uranyl−1,3,5-triazine-2,4,6-triamine hexaacetic acid hybrid materials has been obtained by the reaction of a moderate amount of uranyl acetate dihydrate with the ligands under hydrothermal conditions. Some general trends are worthy of note: first, in the synthetic process of compound **1**, to get the single crystals for X-ray diffraction, we performed a series of experiments using various molar amounts of $UO_2(CH_3COO)_2{\cdot}2H_2O/Nd(NO_3)_3{\cdot}6H_2O/H_6TTHA/4,4'$-bipy under hydrothermal conditions with the addition of the same volume of H_2O. We found that it could be achieved by using the optimal molar amount of 2/1/1/2 mmol. Furthermore, the byproduct resulting from the in situ reaction was obviously decreased. It is surprising to note that, in the reaction of **1**, we have obtained two types of products in the same reaction. One is uranyl compound **1** and the other is lanthanide compound, $[Nd(ox)_{1.5}(H_2O)_3]$ (ox = oxalic acid) as determined by X-ray diffraction. Moreover, research results found that uranyl compound **1** was not repeated without $Nd(NO_3)_3{\cdot}6H_2O$ in the same experimental conditions. It is indicated that the addition of lanthanide nitrate salt has substantial effects on this reaction, and it especially affects crystallization of the compound. Even if it is not incorporated into the initial target product (4f−5f−H_6TTHA), the control of the molar ratio and molar concentration could also affect the crystallization of the compound. Second, the pH plays an important role in the syntheses of uranyl hybrid materials. Considering the attractive symmetry and flexibility of the ligand, more attempts to obtain other compounds with novel topological structures were tried. Thus, further exploration in our group has focused on adjusting the pH value of the reactions through accurate control of the amount of HNO_3. From these results, two polynuclear metal compounds, $\{[(UO_2)_3(TTHA)(H_2O)_3]\}_n$ (**2**) and $\{[(UO_2)_5(TTHA)(HTTHA)(H_2O)_3]{\cdot}H_3O\}_n$ (**3**), were eventually obtained at the different pH values. By X-ray structural analysis, compounds **2** and **3** produced different structural manifestations of the 3D network motif as a main function of the pH. Indeed, for a given temperature, the other influential parameter is the reaction pH. It should be noted that pH was not measured exactly during the hydrothermal treatment although it is possible to estimate its value by using in situ liquid NMR spectroscopy.[28] Nevertheless, the scan of the different pH values before (or after) the reaction is also an approximate probe, which gave us evidence of the pH effect on the structural diversities in the chemical system $[UO_2]^{2+}/H_6TTHA/H_2O$.

Structure Descriptions. Crystallization of H_6TTHA from its aqueous solution yields a solid that can be examined by single-crystal X-ray diffraction, and the same structure has been previously reported.[20e]

*{[$(UO_2)_2(H_2TTHA)(H_2O)$]·4,4′-bipy·$2H_2O$}$_n$ (**1**).* The structure of **1** comprises two crystallographically distinct U^{VI} centers that occur with hexagonal- and pentagonal-bipyramidal coordination geometries (Figure 1). The uranyl oxygen atoms at the apexes are bonded to the central uranium atoms at an average distance of 1.764(4) Å, and the O═U═O bond angles are 176.78(19)° for U1 and 176.98(17)° for U2 to form the near-linear $[UO_2]^{2+}$ cations, which is in good agreement with the reported average uranyl bond length and angle of 1.774(3) Å and 178.5(2)°, respectively.[15d,29a] Six equatorial positions of U1 are occupied by oxygen atoms from three chelating carboxylate groups pertaining to three H_2TTHA^{4-} ligands. Within the pentagonal-bipyramidal coordination sphere of U2, the equatorial girdle is completed by three distinct types of oxygen

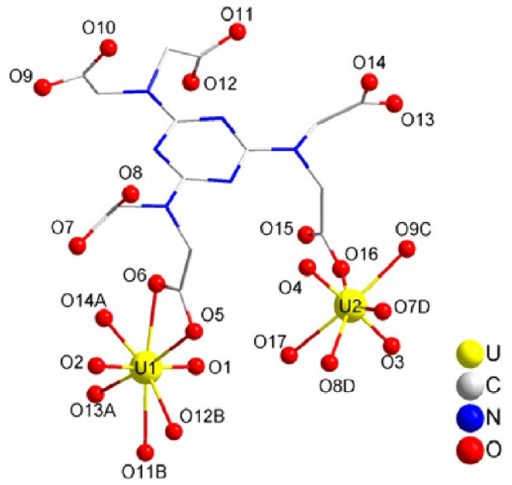

Figure 1. Perspective view of the coordination environment around the uranium atoms in **1**. Hydrogen atoms have been omitted for clarity. Symmetry codes: A, 0.5 + *x*, 1.5 − *y*, 0.5 + *z*; B, 1.5 − *x*, −0.5 + *y*, 1.5 − *z*; C, −1 + *x*, *y*, *z*; D, 1 − *x*, 1 − *y*, 1 − *z*.

atoms from one aqua ligand and one chelating and two monodentate carboxylate groups. The average U−O bond lengths of 2.471(4) Å for chelating and 2.273(4) Å for monodentate groups are unexceptional (average values from the relevant literature: 2.504(10) Å and 2.42(5) Å, respectively).[15h] Furthermore, the bond length of U2−O17 [2.411(4) Å] is also comparable to those $U-O_{(aquo)}$ (<2.41(3) Å>) reported in other uranyl compounds.[15i]

As described above, two coordination modes of the carboxylate groups in the H_2TTHA^{4-} ligand are observed: chelating bidentate and monodentate. The whole ligand is 4-fold deprotonated and acts as a μ_{10}-bridge to link six U^{VI} centers as illustrated in Scheme 2a. Because of its flexibility, six of the $-CH_2(COOH)$ groups (as if arms) show significant deviation from the central triazine ring, and none of them are

Scheme 2. Conformations and Coordination Modes of the Ligand TTHA in (a) Compound 1, (b) Compound 2, and (c) Compound 3

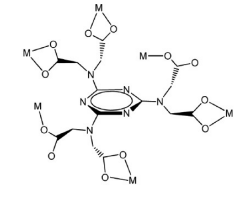

III-2
μ_6-$\eta^1\eta^1\eta^1\eta^1\eta^1\eta^1\eta^1\eta^1\eta^1\eta^1\eta^1\eta^1$
(a)

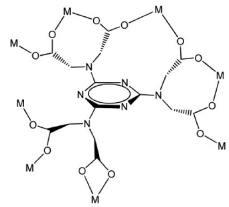

V-5
μ_8-$\eta^1\eta^1\eta^1\eta^1\eta^1\eta^1\eta^1\eta^1\eta^1\eta^1\eta^1\eta^1\eta^1\eta^1$
(b)

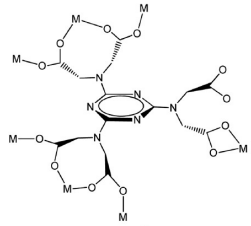

IV-3
μ_7-$\eta^1\eta^1\eta^1\eta^1\eta^1\eta^1\eta^1\eta^1\eta^1\eta^1\eta^1\eta^1$
(c-1)

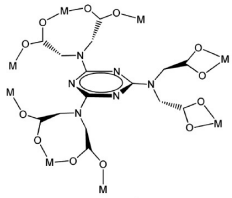

IV-4
μ_8-$\eta^1\eta^1\eta^1\eta^1\eta^1\eta^1\eta^1\eta^1\eta^1\eta^1\eta^1\eta^1\eta^1\eta^1$
(c-2)

DOI: 10.1021/acs.inorgchem.5b01364
Inorg. Chem. 2015, 54, 9046−9059

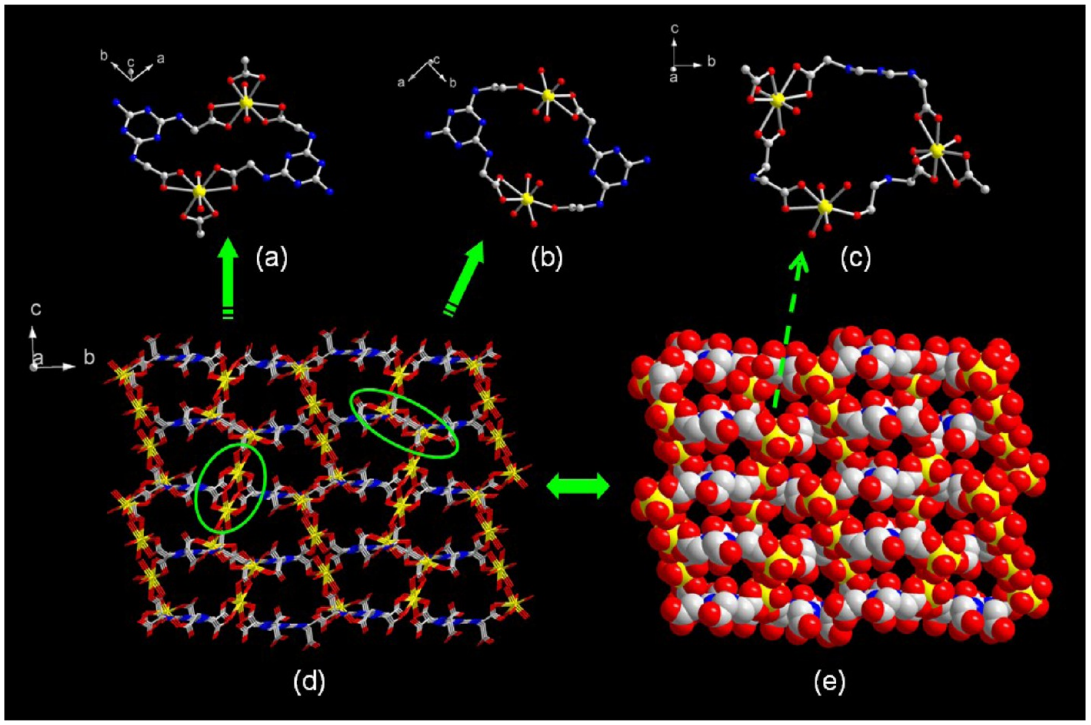

Figure 2. Structure of UOF **1**: (a) view of the first SBU composed of two U1 FBUs; (b) view of the second SBU composed of two U2 FBUs; (c) view of the large channel surrounded by two U1, one U2 FBUs, and six arms along the *a*-axis; (d) view of the 3D network structure viewed in the shape of "matts" type; (e) space-filling representation of the molecular cage with large channels. Hydrogen atoms, solvent molecules, and free 4,4′-bipyridine molecules are omitted for clarity.

coplanar with the triazine ring. The two arms connecting to the same nitrogen atom are arranged above and below the triazine plane. The adjacent arms bend in the same direction when they adopt different coordination modes, whereas in other conditions, the arms bend in opposite directions to the triazine plane, which may reduce the stereospecific blockade. In this way, a fascinating 3D porous framework (Figure 2) has been generated based on two types of SBUs. The first is composed of two U1 FBUs (fundamental building units), which is connected with four arms of the ligand to form a 24-membered ring. Similarly, the second is composed of two U2 FBUs, which is also connected with four arms of the ligand to form a 24-membered ring. Moreover, the large channel with a 28-membered ring (approximately 11.6 × 8.3 $Å^2$ by ignoring the suspending groups), surrounded by two U1 FBUs and one U2 FBU as well as six arms, can be discovered along the *a*-axis. To identify the connectivity between the ligands and the metals, we investigated the topology of the whole network. The two simplified ways of the ligand are illustrated in Figure 3. If the

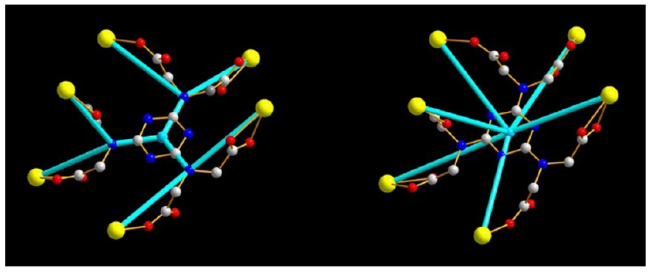

Figure 3. Two simplified ways of the ligand in compound **1** (for these, compounds **2** and **3** are similar to **1**).

two FBUs (U1 and U2), three N_{amine} atoms, and the triazine ring center are viewed as nodes, the compound can be interpreted topologically as a special 3D (3,3,3,3,3,3)-connected 2-nodal net with a Schläfli symbol (8^3). This initial simplification, however, does not interpret the whole network structure in a legible way. Thus, we further simplify the structure by considering the whole H_2TTHA^{4-} ligand as a node. In such a manner, the network is further computed as a (3,3,6)-connected 3-nodal net with a Schläfli symbol of (4.6^2)($4^2.6$)($4^3.6^6.8^6$) (Figure 4).

{[$(UO_2)_3$(TTHA)$(H_2O)_3$]}$_n$ (**2**). As illustrated in Figure 5, the asymmetric unit in compound **2** consists of three crystallographically independent uranyl ions, one completely deprotonated $TTHA^{6-}$ ligand, and three aqua ligands. All of the uranium centers adopt a 7-fold coordinated (pentagonal bipyramid), and terminal short U═O are observed with an unexceptional average bond length of 1.764(9) Å as well as O═U═O angles ranging from 176.6(4)° to 177.0(5)°, which are typical of the double uranyl bond. The oxygen atoms from bridging carboxylate groups and aqua ligands complete the coordination spheres of U1 and U2 and are located in the equatorial plane, whereas that of U3 is completed by three bridging carboxylate oxygen atoms and two chelating carboxylate oxygen atoms. The average $U-O_{(bridging\ carboxylate)}$, $U-O_{(chelating\ carboxylate)}$, and $U-O_{(aqua)}$ bond lengths 2.362(8), 2.478(8), and 2.449(8) Å, respectively, match their counterparts in **1** and other uranyl-oxygen donor compounds ($U-O_{(bridging\ carboxylate)}$ <2.330(3) Å>).[29c]

The carboxylate moieties feature three coordination modes in the $TTHA^{6-}$ ligand, *syn*−*anti* bridging, *anti*−*anti* bridging, and chelating bidentate. The whole ligand functions as a μ_{12}-bridge connecting eight metal centers (Scheme 2b). Interestingly, the ligand in compound **2** exhibits more flexibility than it

DOI: 10.1021/acs.inorgchem.5b01364
Inorg. Chem. 2015, 54, 9046−9059

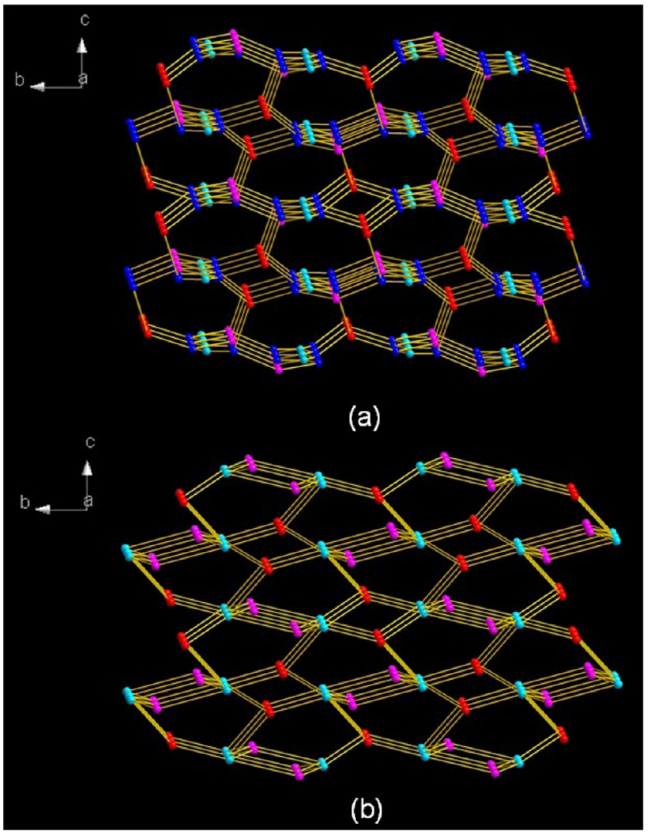

Figure 4. Topological presentation of the 3D net in compound **1**: (a) (3,3,3,3,3,3)-connected 2-nodal net; (b) (3,3,6)-connected 3-nodal net. Red and pink balls represent U1 and U2 FBUs, respectively; blue balls represent the N_{amine} atom, and the turquoise balls represent the triazine ring centers.

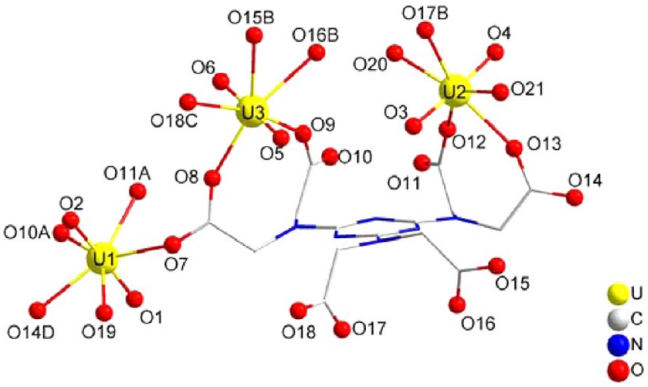

Figure 5. Perspective view of the coordination environment around the uranium atoms in **2**. Hydrogen atoms have been omitted for clarity. Symmetry codes: A, $1 - x$, $0.5 + y$, $0.5 - z$; B, x, $0.5 - y$, $0.5 + z$; C, $-x$, $1 - y$, $-z$; D, x, $1 + y$, z.

does in the former compound, which exhibits the mirror symmetry in itself. Two couples of arms bend in the same direction to the triazine plane, whereas the other couple of arms bend in the opposite direction. In the extended structure (Figure 6), the uranyl ions (U2 and U3) are bridged by the carboxylate groups into an SBU, further forming a two-dimensional crown-like sheet in the *bc* plane through the connection with the ligands. Moreover, the U1 FBUs are bridged by the carboxylate groups into one-dimensional wall-like infinite chains along the *b*-axis, in which nearly planar 16-membered rings are arranged with a U1−U1 contact of 9.5088(27) Å. Finally, the uranyl ion (U1) as a hub connects these 2D sheets to form an intriguing 3D network structure. With topological analysis, if the FBU (U1) and the $[(UO_2)_2(\mu_2\text{-}CO_2)]$ dimer unit (U2/U3) are viewed as 4-connected nodes, whereas three N_{amine} atoms and the triazine ring center act as 3-connected, 4-connected, 4-connected, and 3-connected nodes, respectively, the structure of **2** can be symbolized as an unusual 3D (3,3,4,4,4,4)-connected 6-nodal net topology with a Schläfli symbol of $(4.8^2)(4.8^4.10)(4^3.6^2.8)(4^4.6^2)_2(8^2.10)$. Similarly, the Schläfli symbol $(4.6.8)(4^2.6)(4^3.6^4.8^8)$ for a (3,3,6)-connected 3-nodal net framework can be achieved when the whole $TTHA^{6-}$ ligands are simplified to 6-connected nodes (Figure 7).

{[(UO$_2$)$_5$(TTHA) (HTTHA)(H$_2$O)$_3$]·H$_3$O}$_n$ (**3**). The X-ray crystal structure analysis reveals that compound **3** similarly possesses a 3D network framework. It exhibits unusual structural features for crystal chemistry of uranyl-based solids in which the asymmetric unit comprises five crystallographically independent uranyl ions and two ligands ($HTTHA^{5-}$ and $TTHA^{6-}$). All of the uranium centers are 7-fold coordinated with typical pentagonal-bipyramidal configurations (Figure 8). As expected for these U^{VI}, two double uranyl bonds exist with typical short U═O distances and near-linear O═U═O angles [1.732(14)−1.778(11) Å and 176.8(5)−178.8(6)°, respectively]. Each of them have the same equatorial coordination sphere. In the case of U1 and U4, five oxygen atoms are from one chelating and three bridging carboxylate groups. For U2 and U5, the oxygen atoms are from four bridging carboxylate groups and one aqua molecule, whereas that of U3 is completed by five oxygen atoms from one chelating carboxylate group and two bridging carboxylate groups as well as one aqua ligand, respectively. The U−O distances in the equatorial plane are in the range of 2.317(12)−2.489(11) Å, all of which are unexceptional.

The incompletely and completely deprotonated ligands $HTTHA^{5-}/TTHA^{6-}$ in **3** connect seven and eight different metal centers (μ_{10}- and μ_{12}-bridges), respectively, through *syn*−*anti* bridging, *anti*−*anti* bridging, and chelating bidentate carboxylate moieties (Scheme 2c). For the $TTHA^{6-}$ ligand, the adjacent two couples of arms connecting to N4 and N6 are arranged above and below the triazine plane, respectively, whereas the other two arms connecting to N5 bend in opposite directions to the triazine plane. Similarly, the six arms of the $HTTHA^{5-}$ ligand are arranged in the same way as the former based on the plane of the triazine ring. However, one carboxylate group (C30, O36, and O37) of the $HTTHA^{5-}$ ligand is uncoordinated. As expected, a complicated 3D network structure is formed through continuous symmetric connections that are based on two types of SBUs, the $[(UO_2)_3(\mu_2\text{-}CO_2)_2]$ trimer unit for U1/U4/U5 and the $[(UO_2)_2(\mu_2\text{-}CO_2)]$ dimer unit for U2/U3 connected by bridging carboxylate groups (Figure 9). In consideration of the complexity of the structure, we try to interpret the framework topologically through six N_{amine} atoms, the two triazine ring centers, U1/U4/U5 and U2/U3 building units being defined as nodes. The simplified structure gives an unprecedented (2,3,3,3,3,3,3,3,3,8)-connected 10-nodal net topology with the Schläfli symbol $(4.6.8)(4.8.10)_2(4.8^2)\text{-}(4^2.6)_2(4^3)(4^5.6^7.8^8.10^6.12^2)(6.8^2)(6)$ (Figure 10a). For better insight into such an elegant 10-nodal net, the whole ligands $HTTHA^{5-}$ and $TTHA^{6-}$ are both viewed to be 5- and 4-connected nodes, respectively. Finally, compound **3** shows a

DOI: 10.1021/acs.inorgchem.5b01364
Inorg. Chem. 2015, 54, 9046−9059

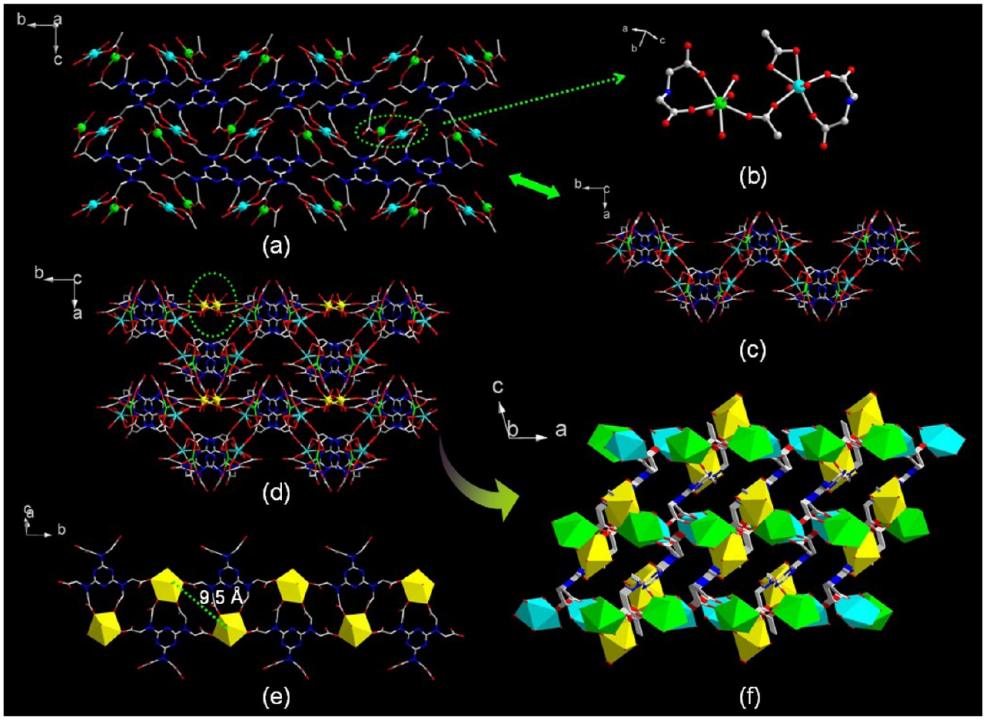

Figure 6. Structure of UOF **2**: (a) view of the two-dimensional sheet in the *bc* plane (the uranyl oxygen atoms of U2 and U3 have been omitted for clarity); (b) view of the SBU; (c) the crown-like sheet viewed side-on; (d) view of another 2D sheet connected by uranyl ions (U1) as hubs in the *ab* plane; (e) view of the 1D wall-like chains along the *b*-axis; (f) view of the 3D network framework. The uranium atoms and uranyl coordination polyhedra are in yellow (U1), bright green (U2), and sky blue (U3). Hydrogen atoms are omitted for clarity.

novel 3D (3,4,5,6)-connected 4-nodal net topology with a Schläfli symbol $(4^2.6)$ $(4^4.6^2)(4^5.6^4.8)(4^8.6^6.8)$ (Figure 10b).

Comparison of TTHA Conformations and Coordination Modes. So far, a series of compounds constructed from the 1,3,5-triazine-2,4,6-triamine hexaacetic acid (H_6TTHA) containing three iminodiacetic acid groups, which can adopt versatile conformations according to the geometric requirements of different metal ions, have been continually reported.[19,20] By a systematic comparison in terms of conformations and coordination modes of the ligand, seven types of TTHA conformations (I → VII) and 24 kinds of coordination modes could be clearly observed (Scheme 3). To our surprise, the ligands of compounds **1**−**3** reported herein exhibit distinctly different coordination modes. In addition, the weaker metal−N_{amine} chelation is prominent in d-block elements like Cu-, Zn-, and Cd-based compounds. Up until now, no such instances have been found with the s- or f-block elements. It may be explained that geometrical constraints, which prefer a certain type of coordination geometry with restrictions on the coordination bond lengths, have a bearing on the outcome of aggregation. Noteworthily, it is quite difficult that the tridentate coordination mode involving the amine N atom is favored with the uranium atom in view of the feature of coordinated sphere for the linear $[UO_2]^{2+}$ cation. That is, the amine N and two O atoms from N−diacetate groups could not accomplish coplanarity with the U^{VI} center owing to the restrictions on the rotary degree of the arms and ranges of bond lengths and angles, especially U−N and U−O. Herein, we adopted the currently approved notation, based on Greek letters μ and η, to describe the bonding modes of the whole TTHA ligand in Schemes 2 and 3.

Infrared Spectroscopy. The synthesized uranyl compounds **1**−**3** were characterized by IR spectra as shown in Figure S2. For **1**, the symmetric and asymmetric stretching vibrations of U═O are observed at approximately 887 and 921 cm^{-1} (842 and 929 cm^{-1} for **2**, 850 and 925 cm^{-1} for **3**). The peaks at 1641 and 1380 cm^{-1} are associated with the O−C−O asymmetric and symmetric stretching vibrations (1598 and 1394 cm^{-1} for **2**, 1621 and 1386 cm^{-1} for **3**). For the three samples, a very broad band is observed around 3200−3600 cm^{-1} and assigned to stretching vibration of O−H from hydroxy or aqua species. The peaks around 2928 and 2850 cm^{-1} are attributed to the $-CH_2-$ stretching modes. The bands between 1400−1600 cm^{-1} are attributed to the skeletal vibrations of the organic aromatic rings. In addition, in the spectra of compound **3**, the weak shoulder peak at ∼1725 cm^{-1} is associated with the uncoordinated carboxylate group. The characteristic band shown at 3081 cm^{-1} in the spectra of compound **1** corresponds to the aromatic C−H stretching vibrations, which are due to the presence of the free 4,4′-bipyridine molecule.

PXRD Analyses. The powder X-ray diffraction data of compounds **1**−**3** were obtained and compared with the corresponding simulated single-crystal diffraction data (Figure S3). The phases of the corresponding compounds are considered as purities owing to the agreement of the peak positions. The different intensity may be due to the preferred orientation of the powder samples.

Thermal Properties. The thermogravimetric curve (Figure S4) of compound **1** shows different weight loss steps. The first event occurring from 216 up to 246 °C is assigned to the departure of two free water molecules and one aqua ligand (obsd: 4.52%; calcd: 4.42%) and indicates that the interactions of these water molecules with the framework are slightly strong, which ends at a somewhat high temperature. From then on, almost no loss is observed until 260 °C, at which temperature

DOI: 10.1021/acs.inorgchem.5b01364
Inorg. Chem. 2015, 54, 9046−9059

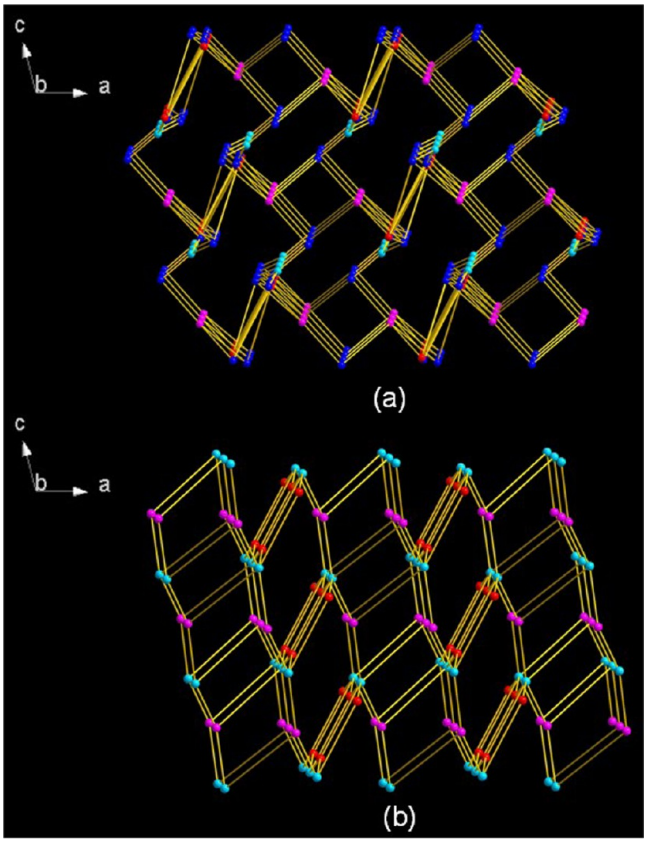

Figure 7. Topological presentation of the 3D net in compound **2**: (a) (3,3,4,4,4,4)-connected 6-nodal net; (b) (3,3,6)-connected 3-nodal net. Red and pink balls represent the FBU (U1) and the $[(UO_2)_2(\mu_2\text{-}CO_2)]$ dimer unit (U2/U3), respectively; blue balls represent the N_{amine} atoms, and turquoise balls represent the triazine ring centers.

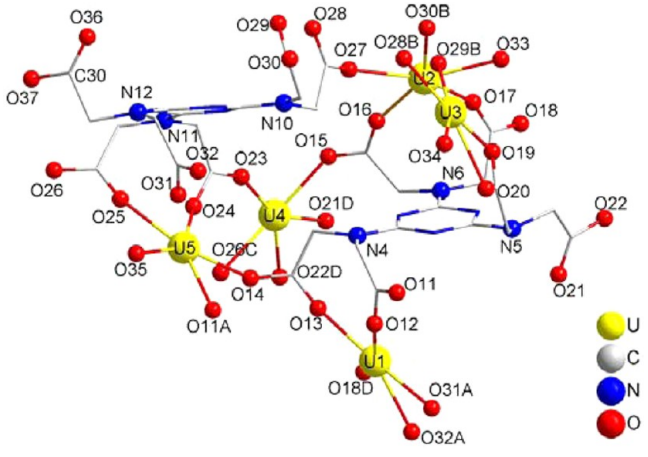

Figure 8. Perspective view of the coordination environment around the uranium atoms in **3**. The uranyl oxygen atoms at the apexes (O1, O2 for U1; O3, O4 for U2; O5, O6 for U3; O7, O8 for U4; O9, O10 for U5) and hydrogen atoms have been omitted for clarity. Symmetry codes: A, $1-x, 1-y, 1-z$; B, $1-x, 2-y, 1-z$; C, $2-x, 1-y, 1-z$; D, $1-x, 1-y, 2-z$.

the compound begins to decompose. The second weight loss step up to 375 °C is attributed to the removal of three N–diacetate groups of the H_2TTHA^{4-} ligand (obsd: 31.96%; calcd: 32.14%). The last event, up to 633 °C, corresponds to the decomposition of the 4,4′-bipy and the triazine ring (obsd: 18.20%; calcd: 19.19%). For compound **2**, an immediate weight loss upon heating is completed from 46 °C up to 122 °C, which can be attributed to the loss of three aqua ligands (obsd: 4.13%; calcd: 4.05%). The rapid weight loss starts at ∼200 °C, up to 540 °C, corresponding to the decomposition of three N–diacetate groups of the $TTHA^{4-}$ ligand (obsd: 29.21%; calcd: 29.29%). The remaining weight loss to 735 °C is in good agreement with further the decomposition of the triazine ring (obsd: 5.68%; calcd: 5.86%). The TGA curve of compound **3** illustrates that there is a significant weight loss stage between 42 and 110 °C due to the loss of the hydronium, three aqua ligands, and the uncoordinated carboxylate group (obsd: 4.95%; calcd: 5.00%) because of the instability of the group as described in the X-ray crystallographic determination section. A rather complicated continuous weight loss profile starts at 200 °C, suggesting decomposition of the organic linkers.

UV–Vis Spectroscopy. The absorbance spectra for these three novel compounds, $UO_2(CH_3COO)_2{\cdot}2H_2O$, and the H_6TTHA ligand were collected. As shown in Figure S5, the characteristic equatorial U–O charge transfer band and axial U═O charge transfer band (vibronic coupling) are observed around 309 and 420 nm for $UO_2(CH_3COO)_2{\cdot}2H_2O$ and 421 nm for compounds **1**–**3**. Moreover, additional absorbance peaks are also observed along with the characteristic uranyl bands at values around 360 nm for the LMCT transition in the spectra of **1**–**3**. The other three absorption peaks appearing at approximately 220, 259, and 320 nm are associated with the $\pi \rightarrow \pi^*$ transition of the ligand, which are in accordance with the absorbance spectrum of H_6TTHA ligand.

Photoluminescent (PL) Properties and Detection for Nitrobenzene. The luminescent properties of U^{VI} are of interest due to potential applications, including photocatalysis. The utilization of $[UO_2]^{2+}$ ions in compounds arranges the metal centers into an extended topology as well as allows for the introduction of chromophoric organic linkers, which could sensitize the $[UO_2]^{2+}$ luminescence. The luminescence of uranyl compounds centered near 520 nm has been known for centuries. The charge-transfer-based emission is vibronically coupled to both bending and stretching modes of the uranyl cation and typically consists of a five-peak spectrum, although far more lines can be observed at low temperature.[30] Denning and his group members have examined in detail these transitions for the solid samples containing the $[UO_2Cl_4]^{2-}$ anion owing to its crystallization in a cubic space group.[31] However, not all uranyl compounds possess luminescent properties, and the mechanisms of the emission from uranyl compounds are most often difficult to explain. As we reported here, unusual luminescent properties have been documented recently for a family of uranyl flexible hexapodal carboxylates. The luminescent spectra for these three novel carboxylate compounds (λ_{ex} = 290 nm), the benchmark compound $UO_2(CH_3COO)_2{\cdot}2H_2O$ (λ_{ex} = 332 nm), and the ligand (λ_{ex} = 262 nm) were collected under the same experimental conditions and procedures and are shown in Figure 11. Five peaks (452, 470, 491, 515, and 538 nm) for **1** and four peaks (452, 470, 491, and 515 nm) for **2** and **3** are observed in the spectra, which all exhibit characterized emission from uranyl cations. These emission peaks correspond to the electronic and vibronic transitions of $S_{11} \rightarrow S_{00}$, $S_{10} \rightarrow S_{0v}$ (v = 0–3) for **1** and $S_{11} \rightarrow S_{00}$, $S_{10} \rightarrow S_{0v}$ (v = 0–2) for **2** and **3**, and the most intense peak is positioned at 470 nm for these three compounds. As for the benchmark compound, the luminescent spectrum shows well-resolved sharp vibronic peaks at 488, 510,

DOI: 10.1021/acs.inorgchem.5b01364
Inorg. Chem. 2015, 54, 9046–9059

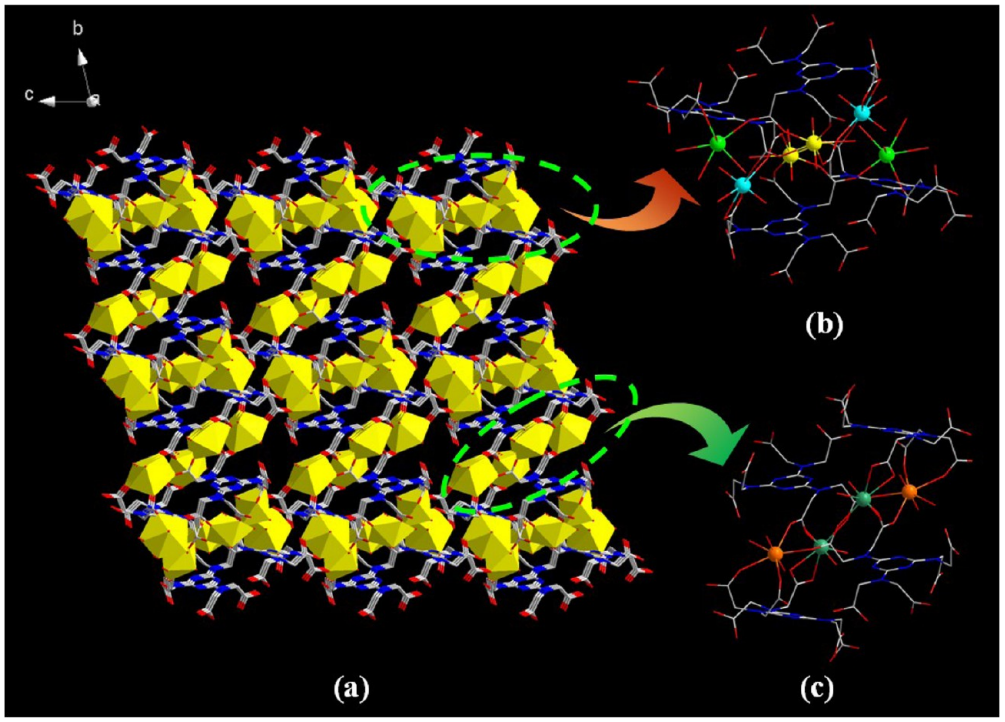

Figure 9. Structure of UOF **3**: (a) view of the 3D framework constructed by two kinds of SBUs (yellow polyhedra) through the linkers $HTTHA^{5-}$/$TTHA^{6-}$; (b) view of one SBU consisting of U1/U4/U5 (U1, U4, and U5 atoms are represented by turquoise, bright green, and yellow spheres, respectively); (c) view of the other SBU consisting of U2/U3 (U2 and U3 atoms are represented by orange and sea green spheres, respectively). Hydrogen atoms and solvent molecules are omitted for clarity.

533, 559, and 587 nm [corresponding to $S_{11} \rightarrow S_{00}$ and $S_{10} \rightarrow S_{0\nu}$ (ν = 0−3)], and the most intense peak ($S_{10} \rightarrow S_{00}$) is positioned at 510 nm. These compounds exhibit a slight blue-shift of 40 nm along with lesser intensity for the emission bands compared to the benchmark compound. Such behaviors were previously observed for other uranyl complexes.[14d,32−34] Moreover, comparison of the observed spectrum for compound **1** to compounds **2** and **3** shows an obvious difference in the shape of the five-peak, which may be attributed to the coordination environment around the uranium centers UO_7 and UO_8 for **1** and UO_7 for **2** and **3**, further resulting in differences in the stereospecific blockade and the symmetry of the uranyl equatorial coordination layer. To our surprise, two additional peaks at 379 and 400 nm were found, corresponding to the $\pi^* \rightarrow \pi$ transition of the ligand and the MLCT transition (from metal to ligand charge transfer transition), respectively, in accordance with the fluorescent spectrum for the ligand (375 and 392 nm). It is indicated that the energy of the ligand does not overall transfer to the $[UO_2]^{2+}$ ions.

To examine the potential of uranyl compounds **1**−**3** toward sensing of small molecules, we investigated its luminescent properties in different solvent emulsions (λ_{ex} = 340 nm). Two milligrams of sample **1** was ground down and then immersed in the corresponding organic solvents (3 mL). After being treated by ultrasonication for 30 min, the samples were suspended in solvents and made into emulsions. The organic solvents used were benzene, DMF, DMSO, chloroform, acetone, ethanol, dichloromethane, and nitrobenzene (Figure 12a). With the unusual luminescent properties of $[UO_2]^{2+}$, it is clear that the different solvents not only altered the PL peak positions but also decreased the emission intensities to different degrees, which were compared with **1** in the solid state. Such solvent-dependent luminescent variation phenomena are largely due to the perturbation of solvent molecules with different polarity and occur within the intermolecular electron-transfer transition between solvent molecules and the UOF framework.[35] The DMF, ethanol, and dichloromethane emulsions display the $\pi^* \rightarrow \pi$ emissions of the ligand at 378 nm and the MLCT transition at 395 nm. The benzene emulsion displays the $\pi^* \rightarrow \pi$ emissions of the ligand at 378 nm, the MLCT transition at 395 nm, and the partial emissions of $[UO_2]^{2+}$ ions at 405, 432, and 461 nm. The chloroform and acetone emulsions display the $\pi^* \rightarrow \pi$ emissions of the ligand at 378 nm and the characterized emissions of $[UO_2]^{2+}$ ions at 405, 432, 461, and 490 nm. For the DMSO emulsion with a large polarity, a broad peak at 441 nm is observed. By controlling the experiments relating the pure ligand and the uranyl group with the DMSO solvent (Figure S6), it could be confirmed that the emission at 441 nm originates from the charge transfer of uranyl cations. In contrast, the nitrobenzene emulsion displays the most obvious quenching effect. The luminescence quenching may be due to the photoinduced electron-transfer mechanism.[24h] The electron-transfer progress can be interpreted by an inductive effect. The LUMO of nitrobenzene is a low-lying π^*-type orbital stabilized by $-NO_2$ through conjugation; thus, it should be lower than LUMO of the ligand and the uranyl cations.[24h] The nitrobenzene with electron-deficient properties can obtain an electron from an excited ligand and uranyl cations. In other words, the excited state electrons can transfer from UOF to nitrobenzene, which leads to luminescence quenching.

The sensing properties of **1** for nitrobenzene were further investigated by monitoring a series of emulsions in DMSO upon gradually increasing the nitrobenzene concentration. As shown in Figure 12b, the luminescence intensity gradually decreases with increasing nitrobenzene concentration. When the concentration of nitrobenzene increased to 1000 ppm, the

DOI: 10.1021/acs.inorgchem.5b01364
Inorg. Chem. 2015, 54, 9046−9059

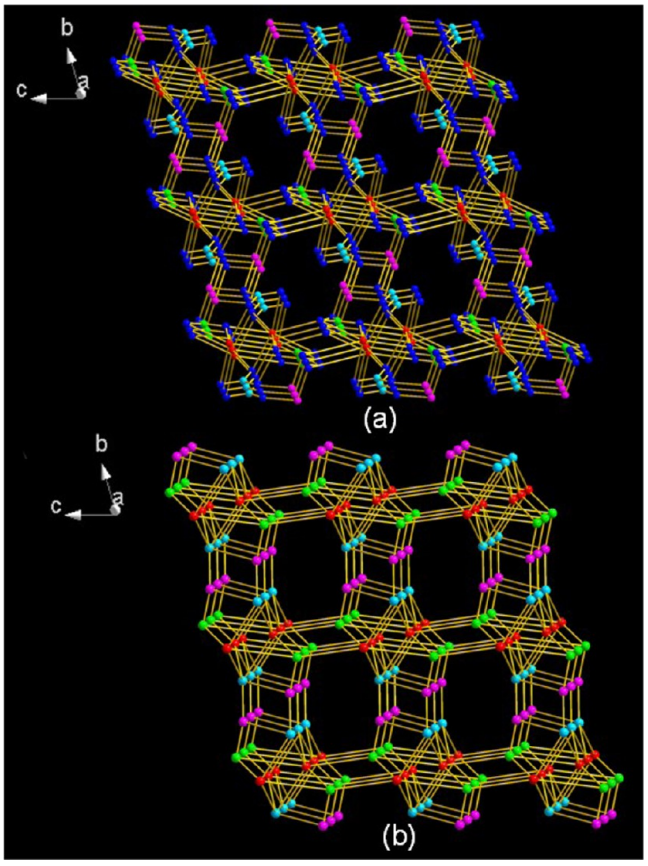

Figure 10. Topological presentation of the 3D net in compound **3**: (a) (2,3,3,3,3,3,3,3,3,8)-connected 10-nodal net; (b) (3,4,5,6)-connected 4-nodal net. Red and pink balls represent U1/U4/U5 and U2/U3 building units, respectively; blue balls represent the N_{amine} atoms, and the turquoise and green balls represent the triazine ring centers of the $HTTHA^{5-}$ and $TTHA^{6-}$ ligands, respectively.

luminescence intensity was quenched with a high quenching efficiency of 90%. Seemingly, $Zn_3(L1)_2(L2)$ (2) {L1 = 4-[3-(4-carboxyphenoxy)-2-[(4-carboxyphenoxy)methyl]-2-methylpropoxy]benzoate, L2 = 1,4-bis(1-imidazolyl)benzene]},[24i] which has a quenching efficiency of 98.91%, is the most sensitive for nitrobenzene detection. Although there is a certain gap between compound **1** and $Zn_3(L1)_2(L2)$ (2) {L1 = 4-[3-(4-carboxyphenoxy)-2-[(4-carboxyphenoxy)methyl]-2-methylpropoxy]benzoate, L2 = 1,4-bis(1-imidazolyl)benzene]}, the result suggests that compound **1** has a good sensitivity in detecting small amounts of nitrobenzene in solution. To further verify the effect of the nitro group on the sensing of nitrobenzene, we measured the emission spectrum of **1** in toluene (Figure 12c). Obviously, the luminescence intensity of the nitrobenzene emulsion was far below those of others in the benzene series. The result reveals that the nitro group is the main cause of the quenching effect. In addition, compounds **2** and **3** also show sensing properties for nitrobenzene (Figures S7). The different quenching efficiencies of compounds **1**−**3** are compared in Figure 12d.

Surface Photoelectric Properties. We all know that the transfer and separation processes of the photoinduced charge carriers (electron−hole pairs) result in the redistribution of surface charges under illumination, which makes the net surface charges (QSS) and the surface band bending decrease; thus, the SPV response (SPS) is generated.[36] Figure S8 shows the effects of band-to-band transitions on the SPV responses of semiconductors.[36b] The detected signal is equivalent to the change in the surface potential barrier under illumination (δV_s). The value is calculated by the equation $\delta V_s = V_s' - V_s^o$, in which V_s^o and V_s' are the surface potential barriers before and after illumination, respectively. The magnitude of the surface potential barrier depends on the number of the net surface charges. By analogy with other metal oxide semiconductors (e.g., ZnO), the uranyl coordination polymer may be regarded as an extended semiconductor with its valence band consisting of the occupied O orbitals, whereas its conduction band consists of the empty metal (U^{VI}) orbitals. The SPS of compound **1** is shown in Figure 13a. Some overlap of signals was fixed after treatment using the Origin7.0 program.[37] By careful differentiation, compound **1** shows three positive SPV responses in the range 300−550 nm. The response band at λ_{max} = 322 nm can be attributed to the $\pi \rightarrow \pi^*$ transition of ligand, whereas the response at λ_{max} = 358 nm is assigned to the LMCT transition (from ligand to metal charge transfer transition). Furthermore, the encouraging response band at ∼418 nm should be the characteristic of uranyl charge transfer in accordance with the UV−vis spectrum. Compounds **2** and **3** also exhibit similar photovoltage properties (Figure S9). Comparing the SPV responses of compounds **1**−**3**, it can be seen that the position of the highest peak about these three compounds is roughly the same, although their intensities are obviously different. This intensity difference is mainly due to the differences in coordination modes of the H_6TTHA ligand, resulting in the different separation efficiencies of the photoinduced carriers. The results of the SPS indicate that not only semiconductors possess photovoltage characteristic but also that some other materials, such as coordination polymers, also can exhibit the photovoltage properties.

As mentioned above, the basic process of semiconductor surface photovoltaic phenomena is that free charge carriers are formed by creating electron−hole pairs via band-to-band transitions after a semiconductor receives the photons of appropriate energy followed by transfer in opposite directions under the built-in electric field (SCR) and/or diffusion in a certain direction within the surface or the bulk such that the net surface charge (QSS) changes. On the basis of the principle of SPS, Wang et al. have developed an electric-field-induced surface photovoltage spectroscopy (EFISPS) technique,[38] which they have used to investigate in depth the photoelectric properties of semiconductors under the effect of an external electric field. When an external direct current electric field is applied to the two sides of a semiconductor under illumination, it drives the photoinduced holes to transfer in the same direction as the added electric field because of the work of external force, whereas the photoinduced electrons are driven to migrate in the opposite direction, indicating that the mobile direction and diffusive distance of the photoinduced charge carriers can be varied. In other words, the external electric field can promote the separation of the photoinduced charge carriers and hence influence the semiconductor surface photovoltaic effect by influencing the distribution of charge carriers. If we apply a positive electric field (the illuminated surface is positive) vertically to the *p*-type semiconductor surface, whose direction is the same as the direction of the built-in field, the separation efficiency of the photoinduced carriers is increased and the intensity of SPV response increases in the original direction. If a negative electric field, whose direction is opposite to that of the built-in field, is applied, the separation

DOI: 10.1021/acs.inorgchem.5b01364
Inorg. Chem. 2015, 54, 9046−9059

Scheme 3. Conformations (Seven Types) and Coordination Modes (24 Kinds) Reported for the Ligand H_6TTHA

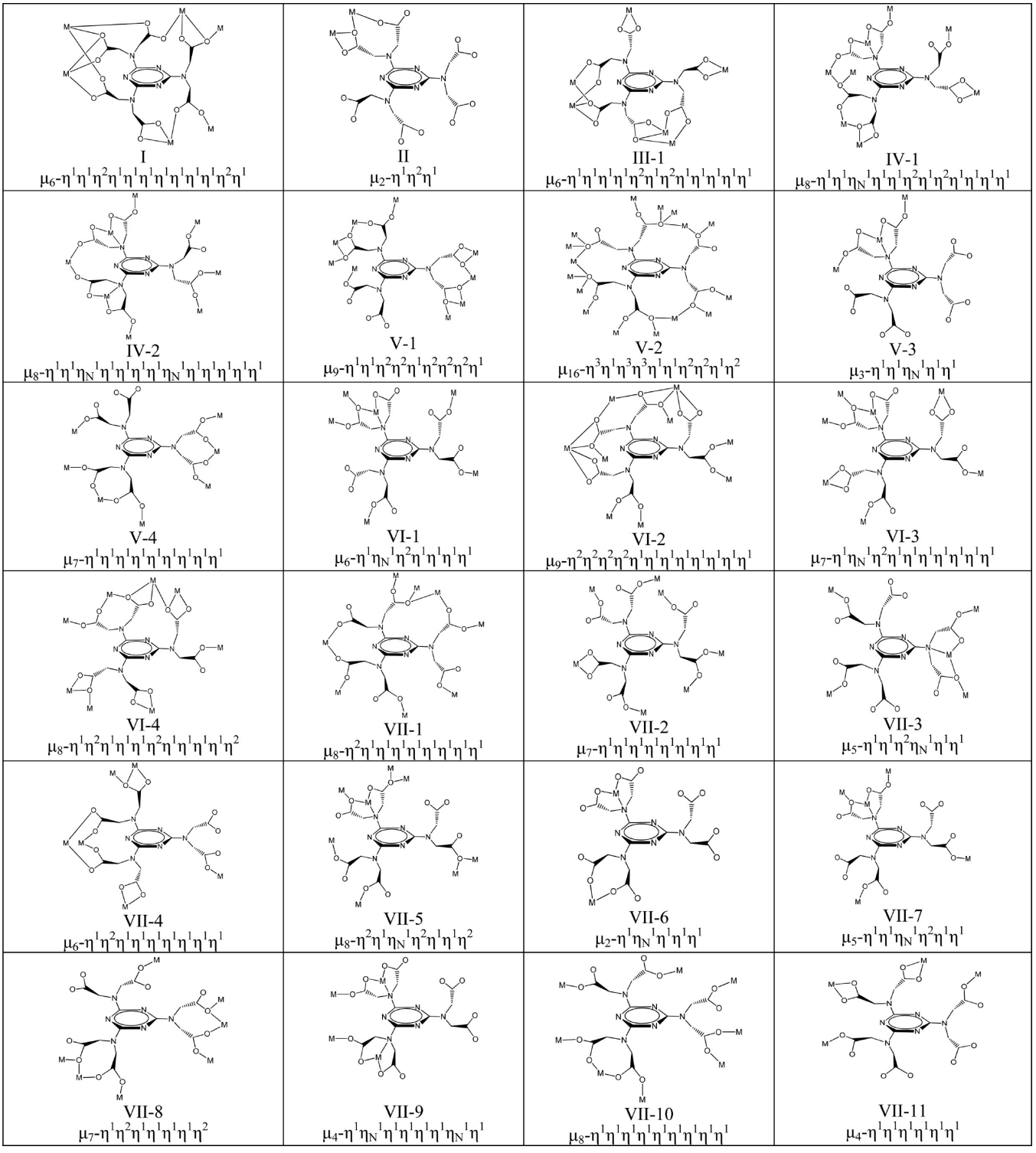

efficiency of the photoinduced carriers reduces and the intensity of the SPV response is weakened, even in the reverse direction. In contrast to *p*-type semiconductors, the SPV response intensity of *n*-type semiconductors increases as a negative field is applied and reduces as a positive electric field is applied. The EFISPS results of compound **1** and compounds **2** and **3** are shown in Figure 13b and Figure S9, respectively. The intensities of the responses are all obviously increased with a positive electric field (+0.2 V) and reduced with a negative electric field (−0.2 V). Hence, it means that compounds **1**−**3** behave as *p*-type semiconductors.

CONCLUSIONS

In this work, a family of uranyl−organic assemblies has been hydrothermally synthesized using the flexible poly(carboxylic acid)s 1,3,5-triazine-2,4,6-triamine hexaacetic acid, which has not previously been reported. Compounds **1**−**3** all exhibit fascinating 3D networks with different topologies resulting

DOI: 10.1021/acs.inorgchem.5b01364
Inorg. Chem. 2015, 54, 9046−9059

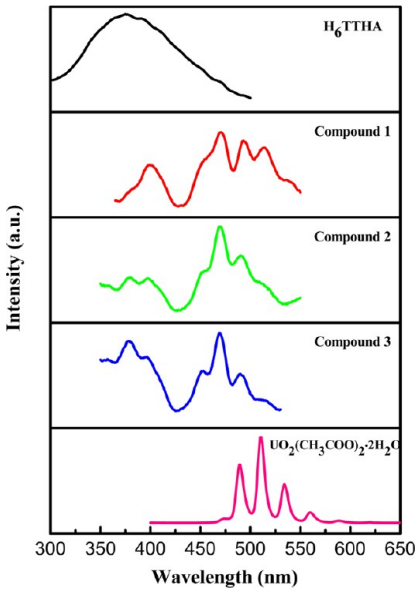

Figure 11. Luminescent spectra of the ligand H_6TTHA (λ_{ex} = 262 nm), $UO_2(CH_3COO)_2{\cdot}2H_2O$ (λ_{ex} = 332 nm), and compounds **1**–**3** (λ_{ex} = 290 nm) in the solid state, showing the green light emission of uranyl centers.

from the different conformations and coordination modes of the flexible ligand, especially displaying structural variation as a function of pH. Luminescence studies were conducted and revealed compound blue-shifted spectra compared to characteristic emissions of uranyl centers. In addition, the coordination environment around the uranium centers could affect the shape

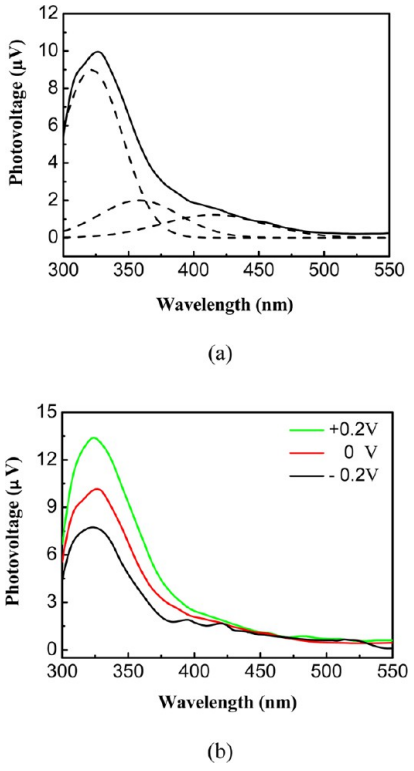

Figure 13. (a) SPS and (b) EFISPS of compound **1**. The dotted lines are the peaks obtained after treatment with the Origin 7.0 program.

of the five-peak by observing and contrasting carefully between emission spectra and the structures of the three uranyl

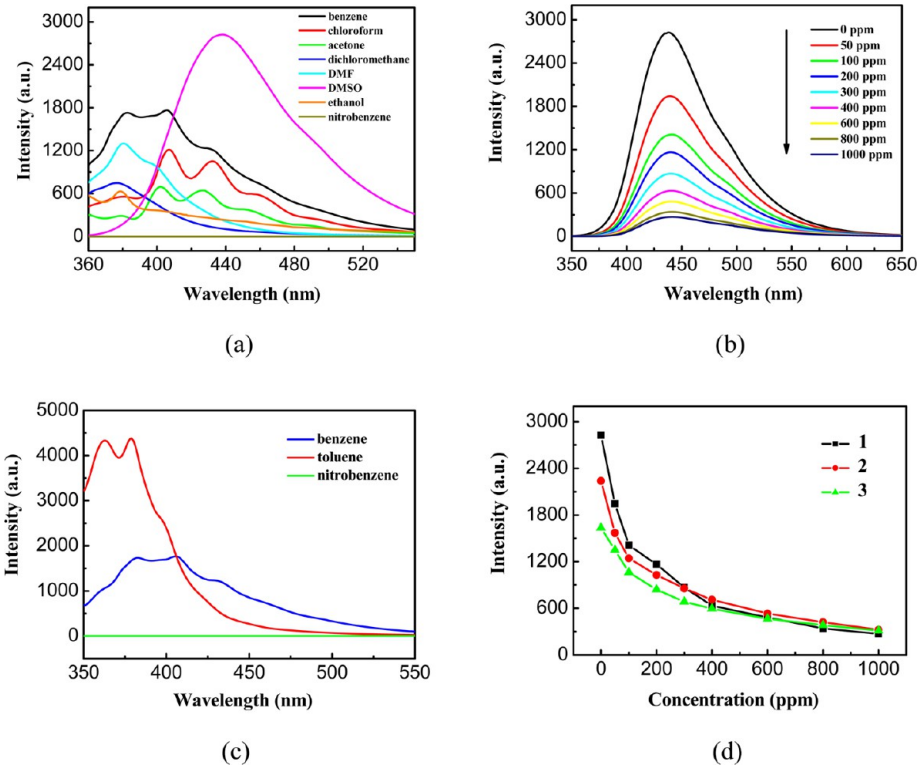

Figure 12. (a) Emission spectra of **1** in different solvents, (b) luminescence quenching of **1** dispersed in DMSO by gradually increasing nitrobenzene concentration, (c) emission spectra of **1** in benzene, toluene, and nitrobenzene, and (d) luminescence quenching efficiencies of compounds **1**–**3** from 0 to 1000 ppm of nitrobenzene concentration.

DOI: 10.1021/acs.inorgchem.5b01364
Inorg. Chem. 2015, 54, 9046−9059

compounds. Furthermore, compounds **1**−**3** display selectivity and sensitivity to nitrobenzene in solution, which may be used for nitrobenzene-sensing applications. The SPS and EFISPS results show that compounds **1**−**3** can behave as *p*-type semiconductors. In summary, the successful syntheses of these compounds and the finding of their unusual physicochemical properties may also help to explore new types of sensing and semiconducting materials, especially among coordination polymers containing actinides. Future efforts will be focused on exploring porous UOF materials with potential applications in highly efficient pollutant removal.

■ ASSOCIATED CONTENT

Supporting Information

The Supporting Information is available free of charge on the ACS Publications website at DOI: 10.1021/acs.inorgchem.5b01364.

Schematic diagram of the photovoltage cell structure, selected bond lengths and angles for compounds **1**−**3**, IR spectra, powder XRD pattern, TG curves, absorption spectra, PL spectra for the H_6TTHA ligand, $UO_2(CH_3COO)_2{\cdot}2H_2O$, and compounds **2**−**3**, the effects of band-to-band transitions on the surface photovoltage responses, SPS and EFISPS for compounds **2**−**3**, and crystallographic data in CIF format for H_6TTHA and compounds **1**−**3** along with CCDC 1058990−1058992 for **1**−**3**, respectively (PDF)

■ AUTHOR INFORMATION

Corresponding Author

*E-mail: xingyongheng2000@163.com.

Notes

The authors declare no competing financial interest.

■ ACKNOWLEDGMENTS

We are grateful for support provided by the National Natural Science Foundation of China (Grant No. 21371086, 21571091), Natural Science Foundation of Guangxi Province (Grant No. 2013GXNSFBA019030), and Commonweal Research Foundation of Liaoning province in China (No. 2014003019).

■ REFERENCES

(1) (a) Doonan, C. J.; Tranchemontagne, D. J.; Glover, T. G.; Hunt, J. R.; Yaghi, O. M. *Nat. Chem.* **2010**, *2*, 235−238. (b) Deng, H. X.; Doonan, C. J.; Furukawa, H.; Ferreira, R. B.; Towne, J.; Knobler, C. B.; Wang, B.; Yaghi, O. M. *Science* **2010**, *327*, 846−850. (c) Dinca, M.; Long, J. R. *Angew. Chem., Int. Ed.* **2008**, *47*, 6766−6779. (d) Rowsell, J. L. C.; Yaghi, O. M. *Angew. Chem., Int. Ed.* **2005**, *44*, 4670−4679.

(2) (a) Liu, Y.; Xuan, W. M.; Cui, Y. *Adv. Mater.* **2010**, *22*, 4112−4135. (b) Li, J. R.; Kuppler, R. J.; Zhou, H. C. *Chem. Soc. Rev.* **2009**, *38*, 1477−1504.

(3) Freudiger, C. W.; Min, W.; Saar, B. G.; Lu, S. J.; Holtom, G. R.; He, C. W.; Tsai, J. C.; Kang, J. X.; Xie, X. S. *Science* **2008**, *322*, 1857−1861.

(4) Andruh, M.; Costes, J. P.; Diaz, C.; Gao, S. *Inorg. Chem.* **2009**, *48*, 3342−3359.

(5) (a) Guo, Y. X.; Feng, X.; Han, T. Y.; Wang, S.; Lin, Z. G.; Dong, Y. P.; Wang, B. *J. Am. Chem. Soc.* **2014**, *136*, 15485−15488. (b) He, Y. C.; Zhang, H. M.; Liu, Y. Y.; Zhai, Q. Y.; Shen, Q. T.; Song, S. Y.; Ma, J. F. *Cryst. Growth Des.* **2014**, *14*, 3174−3178.

(6) (a) Parker, D. *Coord. Chem. Rev.* **2000**, *205*, 109−130. (b) Kuriki, K.; Koike, Y. *Chem. Rev.* **2002**, *102*, 2347−2356. (c) Kido, J.; Okamoto, Y. *Chem. Rev.* **2002**, *102*, 2357−2368.

(7) (a) Nash, K. L. *J. Alloys Compd.* **1994**, *300*, 213−214. (b) Nash, K. L. *J. Alloys Compd.* **1997**, *249*, 33. (c) Jensen, M. P.; Beitz, J. V.; Rogers, R. D.; Nash, K. L. *J. Chem. Soc., Dalton Trans.* **2000**, *18*, 3058−3064.

(8) (a) Shvareva, T. Y.; Almond, P. M.; Albrecht-Schmitt, T. E. *J. Solid State Chem.* **2005**, *178*, 499−504. (b) Shvareva, T. Y.; Sullens, T. A.; Shehee, T. C.; Albrecht-Schmitt, T. E. *Inorg. Chem.* **2005**, *44*, 300−305. (c) Ok, K. M.; Baek, J.; Halasyamani, P. S. *Inorg. Chem.* **2006**, *45*, 10207−10214. (d) Grohol, D.; Blinn, E. L. *Inorg. Chem.* **1997**, *36*, 3422−3428.

(9) (a) Frisch, M.; Cahill, C. L. *Dalton Trans.* **2006**, *39*, 4679−4690. (b) Cahill, C. L.; de Lill, D. T.; Frisch, M. *CrystEngComm* **2007**, *9*, 15−26.

(10) (a) Sykora, R. E.; King, J. E.; Illies, A. J.; Albrecht-Schmitt, T. E. *J. Solid State Chem.* **2004**, *117*, 1717−1722. (b) Liao, Z. L.; Li, G. D.; Bi, M. H.; Chen, J. S. *Inorg. Chem.* **2008**, *47*, 4844−4853. (c) Yu, Z. T.; Liao, Z. L.; Jiang, Y. S.; Li, G. H.; Chen, J. S. *Chem. - Eur. J.* **2005**, *11*, 2642−2650. (d) Xu, X. T.; Hou, Y. N.; Wei, S. Y.; Zhang, X. X.; Bai, F. Y.; Sun, L. X.; Shi, Z.; Xing, Y. H. *CrystEngComm* **2015**, *17*, 642−652.

(11) (a) Baker, R. J. *Chem. - Eur. J.* **2012**, *18*, 16258−16271. (b) Thuéry, P.; Masci, B. *CrystEngComm* **2012**, *14*, 131−137. (c) Thuéry, P. *CrystEngComm* **2012**, *14*, 3363−3366. (d) Adelani, P. O.; Burns, P. C. *Inorg. Chem.* **2012**, *51*, 11177−11183.

(12) (a) Andrews, M. B.; Cahill, C. L. *Chem. Rev.* **2013**, *113*, 1121−1136. (b) Qiu, J.; Burns, P. C. *Chem. Rev.* **2013**, *113*, 1097−1120. (c) Thuéry, P. *Cryst. Growth Des.* **2010**, *10*, 2061−2063.

(13) (a) Sessler, J. L.; Melfi, P. J.; Pantos, G. D. *Coord. Chem. Rev.* **2006**, *250*, 816−843. (b) Jones, M. B.; Gaunt, A. J. *Chem. Rev.* **2013**, *113*, 1137−1198. (c) Mihalcea, I.; Volkringer, C.; Henry, N.; Loiseau, T. *Inorg. Chem.* **2012**, *51*, 9610−9618. (d) Napoline, J. W.; Kraft, S. J.; Matson, E. M.; Fanwick, P. E.; Bart, S. C.; Thomas, C. M. *Inorg. Chem.* **2013**, *52*, 12170−12177. (e) Loiseau, T.; Mihalcea, I.; Henry, N.; Volkringer, C. *Coord. Chem. Rev.* **2014**, *266*−*267*, 69−109.

(14) (a) Chen, W.; Yuan, H. M.; Wang, J. Y.; Liu, Z. Y.; Xu, J. J.; Yang, M.; Chen, J. S. *J. Am. Chem. Soc.* **2003**, *125*, 9266−9267. (b) Wang, K. X.; Chen, J. S. *Acc. Chem. Res.* **2011**, *44*, 531−540. (c) Wu, H. Y.; Wang, R. X.; Yang, W. T.; Chen, J. L.; Sun, Z. M.; Li, J.; Zhang, H. J. *Inorg. Chem.* **2012**, *51*, 3103−3107. (d) Yang, W. T.; Wu, H. Y.; Wang, R. X.; Pan, Q. J.; Sun, Z. M.; Zhang, H. J. *Inorg. Chem.* **2012**, *51*, 11458−11465. (e) Tian, T.; Yang, W. T.; Wang, H.; Dang, S.; Pan, Q. J.; Sun, Z. M. *Inorg. Chem.* **2013**, *52*, 7100−7106. (f) Yang, W. T.; Tian, T.; Wu, H. Y.; Pan, Q. J.; Dang, S.; Sun, Z. M. *Inorg. Chem.* **2013**, *52*, 2736−2743. (g) Zhai, X. S.; Zhu, W. G.; Xu, W.; Huang, Y. J.; Zheng, Y. Q. *CrystEngComm* **2015**, *17*, 2376−2388. (h) Wang, S.; Alekseev, E. V.; Ling, J.; Liu, G.; Depmeier, W.; Albrecht-Schmitt, T. E. *Chem. Mater.* **2010**, *22*, 2155−2163. (i) Alsobrook, A. N.; Hauser, B. G.; Hupp, J. T.; Alekseev, E. V.; Depmeier, W.; Albrecht-Schmitt, T. E. *Chem. Commun.* **2010**, *46*, 9167−9169. (j) Gao, X.; Wang, C.; Shi, Z. F.; Song, J.; Bai, F. Y.; Wang, J. X.; Xing, Y. H. *Dalton Trans.* **2015**, *44*, 11562−11571. (k) Liao, Z. L.; Li, G. D.; Wei, X.; Yu, Y.; Chen, J. S. *Eur. J. Inorg. Chem.* **2010**, *2010*, 3780−3788.

(15) (a) Thuéry, P. *CrystEngComm* **2008**, *10*, 1126−1128. (b) Thuéry, P. *CrystEngComm* **2009**, *11*, 2319−2325. (c) Thuéry, P. *CrystEngComm* **2012**, *14*, 6369−6373. (d) Masci, B.; Thuéry, P. *Cryst. Growth Des.* **2008**, *8*, 1689−1696. (e) Thuéry, P.; Masci, B. *Cryst. Growth Des.* **2010**, *10*, 716−725. (f) Cantos, P. M.; Cahill, C. L. *Cryst. Growth Des.* **2014**, *14*, 3044−3053. (g) de Groot, J.; Gojdas, K.; Unruh, D. K.; Forbes, T. Z. *Cryst. Growth Des.* **2014**, *14*, 1357−1365. (h) Go, Y. B.; Wang, X. Q.; Jacobson, A. J. *Inorg. Chem.* **2007**, *46*, 6594−6600. (i) Thuéry, P. *CrystEngComm* **2009**, *11*, 1081−1088.

(16) Wang, S. N.; Bai, J. F.; Li, Y. Z.; Pan, Y.; Scheer, M.; You, X. Z. *CrystEngComm* **2007**, *9*, 1084−1095.

(17) Wang, S. N.; Sun, R.; Wang, X. S.; Li, Y. Z.; Pan, Y.; Bai, J. F.; Scheer, M.; You, X. Z. *CrystEngComm* **2007**, *9*, 1051−1061.

(18) Han, Z. B.; Zhang, G. X.; Zeng, M. H.; Yuan, D. Q.; Fang, Q. R.; Li, J. R.; Ribas, J.; Zhou, H. C. *Inorg. Chem.* **2010**, *49*, 769−771.

(19) (a) Zhu, Q. L.; Sheng, T. L.; Fu, R. B.; Hu, S. M.; Chen, J. S.; Xiang, S. C.; Shen, C. J.; Wu, X. T. *Cryst. Growth Des.* **2009**, *9*, 5128−

DOI: 10.1021/acs.inorgchem.5b01364
Inorg. Chem. 2015, 54, 9046−9059

5134. (b) Zhu, Q. L.; Sheng, T. L.; Fu, R. B.; Hu, S. M.; Shen, C. J.; Ma, X.; Wu, X. T. *CrystEngComm* **2011**, *13*, 2096−2105. (c) Goswami, P. K.; Singh, M.; Thaimattam, R.; Ramanan, A. *CrystEngComm* **2013**, *15*, 9787−9797. (d) Jiang, X.; Xia, H.; Zhu, Y. F.; Huang, C. X.; Liao, Y. H. *Z. Anorg. Allg. Chem.* **2011**, *637*, 2273−2277. (e) Han, S. D.; Song, W. C.; Zhao, J. P.; Yang, Q.; Liu, S. J.; Li, Y.; Bu, X. H. *Chem. Commun.* **2013**, *49*, 871−873. (f) Jiang, X.; Tao, B.; Xia, H.; Liao, G. Y. *CrystEngComm* **2012**, *14*, 3271−3282.

(20) (a) Zhu, Q. L.; Sheng, T. L.; Fu, R. B.; Hu, S. M.; Chen, L.; Shen, C. J.; Ma, X.; Wu, X. T. *Chem. - Eur. J.* **2011**, *17*, 3358−3362. (b) Jiang, X.; Tao, B.; Xia, H.; Liao, G. Y. *CrystEngComm* **2012**, *14*, 3271−3282. (c) Zhu, Q. L.; Sheng, T. L.; Tan, C. H.; Hu, S. M.; Fu, R. B.; Wu, X. T. *Inorg. Chem.* **2011**, *50*, 7618−7624. (d) Jiang, X.; Lin, L.; Zhu, Y. F.; Xia, H. *Transition Met. Chem.* **2011**, *36*, 901−906. (e) Acharya, S. N. G.; Gopalan, R. S.; Kulkarni, G. U.; Venkatesan, K.; Bhattacharya, S. *Chem. Commun.* **2000**, 1351−1352. (f) Jiang, X.; Yan, G.; Liao, Y. H.; Huang, C. X.; Xia, H. *Inorg. Chem. Commun.* **2011**, *14*, 1924−1927. (g) Zhang, H.; Ma, J. G.; Chen, D. M.; Zhou, J. M.; Zhang, S. W.; Shi, W.; Cheng, P. *J. Mater. Chem. A* **2014**, *2*, 20450−20453.

(21) (a) Salinas, Y.; Martinez-Manez, R.; Marcos, M. D.; Sancenon, F.; Castero, A. M.; Parra, M.; Gil, S. *Chem. Soc. Rev.* **2012**, *41*, 1261−1296. (b) Germain, M. E.; Knapp, M. J. *Chem. Soc. Rev.* **2009**, *38*, 2543−2555.

(22) (a) Boyd, S. A.; Sheng, G.; Teppen, B. J.; Johnston, C. T. *Environ. Sci. Technol.* **2001**, *35*, 4227−4234. (b) Cronin, M. T.; Gregory, B. W.; Schultz, T. W. *Chem. Res. Toxicol.* **1998**, *11*, 902−908. (c) Majumder, P. S.; Gupta, S. K. *Water Res.* **2003**, *37*, 4331−4336.

(23) (a) Czarnik, A. W. *Nature* **1998**, *394*, 417−418. (b) Moore, D. S. *Rev. Sci. Instrum.* **2004**, *75*, 2499−2512.

(24) (a) Dang, S.; Min, X.; Yang, W.; Yi, F. Y.; You, H.; Sun, Z. M. *Chem. - Eur. J.* **2013**, *19*, 17172−17179. (b) Nagarkar, S. S.; Joarder, B.; Chaudhari, A. K.; Mukherjee, S.; Ghosh, S. K. *Angew. Chem., Int. Ed.* **2013**, *52*, 2881−2885. (c) Zhou, X.; Li, H.; Xiao, H.; Li, L.; Zhao, Q.; Yang, T.; Zuo, J.; Huang, W. *Dalton Trans.* **2013**, *42*, 5718−5723. (d) Tian, D.; Li, Y.; Chen, R. Y.; Chang, Z.; Wang, G. Y.; Bu, X. H. *J. Mater. Chem. A* **2014**, *2*, 1465−1470. (e) Pramanik, S.; Hu, Z.; Zhang, X.; Zheng, C.; Kelly, S.; Li, J. *Chem. - Eur. J.* **2013**, *19*, 15964−15971. (f) Wang, G. Y.; Song, C.; Kong, D. M.; Ruan, W. J.; Chang, Z.; Li, Y. *J. Mater. Chem. A* **2014**, *2*, 2213−2220. (g) Qin, J. S.; Bao, S. J.; Li, P.; Xie, W.; Du, D. Y.; Zhao, L.; Lan, Y. Q.; Su, Z. M. *Chem. - Asian J.* **2014**, *9*, 749−753. (h) He, Y. C.; Zhang, H. M.; Liu, Y. Y.; Zhai, Q. Y.; Shen, Q. T.; Song, S. Y.; Ma, J. F. *Cryst. Growth Des.* **2014**, *14*, 3174−3178. (i) Guo, M.; Sun, Z. M. *J. Mater. Chem.* **2012**, *22*, 15939−15946.

(25) Hoog, P. D.; Gamez, P.; Driessen, W. L.; Reedijk, J. *Tetrahedron Lett.* **2002**, *43*, 6783−6786.

(26) Sheldrick, G. M. *SADABS, Program for Empirical Absorption Correction for area Detector Data*; University of Gottingen: Gottingen, Germany, 1996.

(27) Sheldrick, G. M. *SHELXS 97*, program for crystal structure refinement; University of Gottingen: Gottingen, Germany, 1997.

(28) (a) Taulelle, F.; Haouas, M.; Gerardin, C.; Estournes, C.; Loiseau, T.; Ferey, G. *Colloids Surf., A* **1999**, *158*, 299−311. (b) Gerardin, C.; In, M.; Allouche, L.; Taulelle, F. *Chem. Mater.* **1999**, *11*, 1285−1292.

(29) (a) Thuéry, P. *Cryst. Growth Des.* **2011**, *11*, 2606−2620. (b) Diwu, J.; Albrecht-Schmitt, T. E. *Chem. Commun.* **2012**, *48*, 3827−3829. (c) Mihalcea, I.; Henry, N.; Bousquet, T.; Volkringer, C.; Loiseau, T. *Cryst. Growth Des.* **2012**, *12*, 4641−4648.

(30) (a) Liu, G.; Beitz, J. V. In *The Chemistry of the Actinide and Transactinide Elements*; Morss, L. R., Edelstein, N. M., Fuger, J., Eds.; Springer: Heidelberg, 2006; p 2088. (b) Adelani, P. O.; Albrecht-Schmitt, T. E. *Cryst. Growth Des.* **2011**, *11*, 4676−4683.

(31) Denning, R. G.; Norris, J. O. W.; Short, I. G.; Snellgrove, T. R.; Woodwark, D. R. *Lanthanide and Actinide Chemistry and Spectroscopy*; ACS Symp. Ser. No. 131; American Chemical Society: Washington, DC, 1980.

(32) (a) Tian, T.; Yang, W. T.; Pan, Q. J.; Sun, Z. M. *Inorg. Chem.* **2012**, *51*, 11150−11154. (b) Yang, W. T.; Dang, S.; Wang, H.; Tian, T.; Pan, Q. J.; Sun, Z. M. *Inorg. Chem.* **2013**, *52*, 12394−12402.

(33) (a) Frisch, M.; Cahill, C. L. *Dalton Trans.* **2005**, 1518−1523. (b) Harrowfield, J. M.; Lugan, N.; Shahverdizadeh, G. H.; Soudi, A. A.; Thuéry, P. *Eur. J. Inorg. Chem.* **2006**, *2006*, 389−396. (c) Klonkowski, A. M.; Lis, S.; Pietraszkiewicz, M.; Hnatejko, Z.; Czarnobaj, K.; Elbanowski, M. *Chem. Mater.* **2003**, *15*, 656−663. (d) Bunzli, J.-C. G.; Piguet, C. *Chem. Soc. Rev.* **2005**, *34*, 1048−1077. (e) Bunzli, J.-C. G. *Acc. Chem. Res.* **2006**, *39*, 53−61.

(34) (a) Borkowski, L. A.; Cahill, C. L. *Cryst. Growth Des.* **2006**, *6*, 2241−2247. (b) Borkowski, L. A.; Cahill, C. L. *Cryst. Growth Des.* **2006**, *6*, 2248−2259.

(35) (a) Mallick, A.; Garai, B.; Addicoat, M. A.; Petkov, P.; Heine, T.; Banerjee, R. *Chem. Sci.* **2015**, *6*, 1420−1425. (b) Wang, X. M.; Fan, R. Q.; Qiang, L. S.; Wang, P.; Yang, Y. L.; Wang, Y. L. *Dalton Trans.* **2014**, *43*, 16152−16155. (c) Liu, S.; Xiang, Z. G.; Hu, Z.; Zheng, X. P.; Cao, D. P. *J. Mater. Chem.* **2011**, *21*, 6649−6653.

(36) (a) Kronik, L.; Shapira, Y. *Surf. Sci. Rep.* **1999**, *37*, 1−206. (b) Jing, L. Q.; Sun, X. J.; Shang, J.; Cai, W. M.; Xu, Z. L.; Du, Y. G.; Fu, H. G. *Sol. Energy Mater. Sol. Cells* **2003**, *79*, 133−151. (c) Wang, P.; Xie, T. F.; Li, H. Y.; Peng, L.; Zhang, Y.; Wu, T. S.; Pang, S.; Zhao, Y. F.; Wang, D. J. *Chem. - Eur. J.* **2009**, *15*, 4366−4372.

(37) Cao, Y. A.; Meng, Q. J.; Yang, W. S.; Yao, J. H.; Shu, Y. C.; Wang, W.; Chen, G. H. *Colloids Surf., A* **2005**, *262*, 181−186.

(38) (a) Zhang, J.; Wang, D. J.; Shi, T. S.; Wang, B. H.; Sun, J. Z.; Li, T. J. *Thin Solid Films* **1996**, *284/285*, 596−599. (b) Mao, H. F.; Tian, H. J.; Hou, Q. F.; Xu, H. J. *Thin Solid Films* **1997**, *300*, 208−212. (c) Sun, L. P.; Niu, S. Y.; Jin, J.; Yang, G. D.; Ye, L. *Eur. J. Inorg. Chem.* **2006**, *2006*, 5130−5137. (d) Hou, Y. N.; Xu, X. T.; Xing, N.; Bai, F. Y.; Duan, S. B.; Sun, Q.; Wei, S. Y.; Shi, Z.; Zhang, H. Z.; Xing, Y. H. *ChemPlusChem* **2014**, *79*, 1304−1315. (e) Hou, Y. N.; Wang, Z. N.; Bai, F. Y.; Guan, Q. L.; Wang, X.; Zhang, R.; Xing, Y. H. *RSC Adv.* **2014**, *4*, 21180−21189. (f) Lu, Y. C.; Wang, L. L.; Wang, D. J.; Xie, T. F.; Chen, L. P.; Lin, Y. H. *Mater. Chem. Phys.* **2011**, *129*, 281−287.

DOI: 10.1021/acs.inorgchem.5b01364
Inorg. Chem. 2015, 54, 9046−9059